ADVANCED PHYSICS RESEARCH Open Access
www.advphysicsres.com

Elucidating the Role of Dimensionality on the Electronic Structure of the Van der Waals Antiferromagnet $NiPS_3$

Michael F. DiScala, Daniel Staros, Alberto de la Torre, Annette Lopez, Deniz Wong, Christian Schulz, Maciej Barkowiak, Valentina Bisogni, Jonathan Pelliciari, Brenda Rubenstein, and Kemp W. Plumb**

The sustained interest in investigating magnetism in the 2D limit of insulating antiferromagnets is driven by the possibilities of discovering, or engineering, novel magnetic phases through layer stacking. However, due to the difficulty of directly measuring magnetic interactions in 2D antiferromagnets, it is not yet understood how *intra*layer magnetic interactions in *insulating*, strongly correlated, materials can be modified through layer proximity. Herein, the impact of reduced dimensionality in the model van der Waals antiferromagnet $NiPS_3$ is explored by measuring electronic excitations in exfoliated samples using Resonant Inelastic X-ray Scattering (RIXS). The resulting spectra shows systematic broadening of NiS_6 multiplet excitations with decreasing layer count from bulk down to three atomic layers (3L). It is shown that these trends originate from a decrease in transition metal-ligand and ligand–ligand hopping integrals, and by charge-transfer energy evolving from $\Delta = 0.83$ eV in the bulk to 0.37 eV in 3L $NiPS_3$. Relevant intralayer magnetic exchange integrals computed from the electronic parameters exhibit a decrease in the average interaction strength with thickness. This study underscores the influence of *inter*layer electronic interactions on *intra*layer ones in insulating magnets, indicating that magnetic Hamiltonians in few-layer insulating magnets can greatly deviate from their bulk counterparts.

1. Introduction

In 2D magnets, enhanced fluctuations and lattice connectivity strike a balance from which collective states unobtainable in three dimensions may emerge. The ability to prepare isolated monolayers of van der Waals (vdW) magnets has enabled access to new magnetic phases and tests of fundamental theorems of magnetism,[1–6] and opens up possibilities for controlling or engineering unconventional states through stacking.[7] Much work has concentrated on vdW materials with a net ferromagnetism in the 2D limit.[5,8–10] However, antiferromagnets may offer more possibilities to explore complex magnetic order, topological spin textures, or quantum spin-liquids that arise from frustrated interactions and which are stabilized in 2D.[11–15]

$NiPS_3$ stands as one of the few exfoliatable materials that exhibits both antiferromagnetic order and strong correlations.[16,17] Recent Raman scattering measurements suggest that the magnetic order in $NiPS_3$ is highly sensitive to dimensionality and find that long-range order vanishes in the monolayer limit in favor of a fluctuating magnetic phase.[3] Based on the magnetic Hamiltonian that was determined by inelastic neutron scattering on bulk samples,[18] the thickness-dependent Raman data were associated with the proliferation of vorticies through a Berezinskii–Kosterlitz–Thouless phase transition in the 2D material.

M. F. DiScala, A. de la Torre, A. Lopez, K. W. Plumb
Department of Physics
Brown University
Providence, RI 02912, USA
E-mail: kemp_plumb@brown.edu

D. Staros, B. Rubenstein
Department of Chemistry
Brown University
Providence, RI 02912, USA
E-mail: brenda_rubenstein@brown.edu

D. Wong, C. Schulz, M. Barkowiak
Department of Dynamics and Transport in Quantum Materials
Helmholtz-Zentrum Berlin für Materialen und Energie
Albert-Einstein-Strasse 15, 12489 Berlin, Germany

V. Bisogni, J. Pelliciari
National Synchrotron Light Source II
Brookhaven National Laboratory
Upton, NY 11973, USA

The ORCID identification number(s) for the author(s) of this article can be found under https://doi.org/10.1002/apxr.202300096

DOI: 10.1002/apxr.202300096

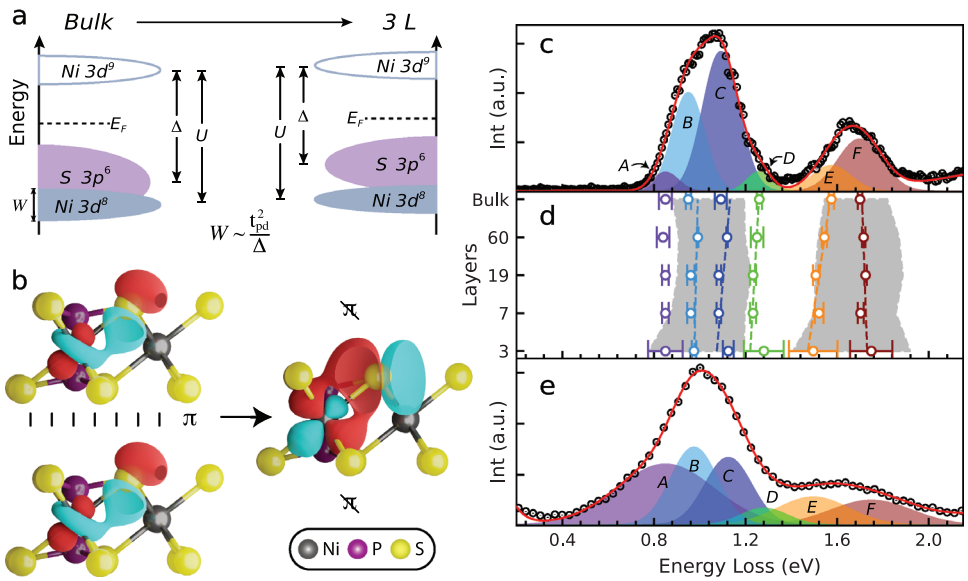

Figure 1. a) Schematic electronic density of states from bulk to 3L $NiPS_3$. b) Visualization of the change in the overlap between MWLFs with dominant contribution to Ni-S hopping integrals from bulk (left) to 1L (right) $NiPS_3$ due to the loss of π-like vdW interactions. Figure was created using both VESTA and Blender software packages.[19,20] Bulk (c) and 3L (e) $NiPS_3$ RIXS sepctra at Ni L_3-edge. Black points are experimental data with errorbars smaller than the symbol size, red lines show Gaussian fit to the data. d) Gaussian peak position versus layer count. Dashed linear fits highlight the electronic structure change with thickness; gray regions follow the numerical center of mass and full width half max of the overall experimental peaks.

However, this explanation assumes that the few-layer magnetic Hamiltonian is identical to that in the bulk. More direct experimental access to the electronic energy scales and magnetic interactions is thus necessary to resolve the nature of the magnetic state in exfoliated $NiPS_3$.

In this work, we demonstrate that Ni-S electronic energy scales are strongly altered by dimensionality in $NiPS_3$ leading to a few-layer magnetic Hamiltonian that differs from that of the bulk. We use resonant Inelastic X-ray Scattering (RIXS) to directly interrogate correlated electronic states in exfoliated flakes of $NiPS_3$ and reveal a systematic softening and broadening of NiS_6 multiplet excitations with decreasing thickness that is reproduced by a multiplet ligand-field model. Overall, we find that decreased hopping integrals and charge transfer energy in 2D result in a more covalent character for Ni d-orbitals (**Figure** 1a). We additionally compute the relevant magnetic exchange integrals and find a decrease in the second- and third-nearest neighbor magnetic interaction strengths, and an increase in the first-nearest neighbor interaction strength. This change moves $NiPS_3$ closer to the boundary between the stripy antiferromagnetic and spiral ordered phases of the honeycomb antiferromagnet. Lastly, we show how the change of electronic energy scales in thinner samples occurs due to decreased electronic vdW delocalization across layers in the 2D limit. Since this mechanism is not necessarily specific to $NiPS_3$, its effect will be important to the properties of a broad class of strongly correlated few-layer vdW magnets.

2. Experimental Results

$NiPS_3$ crystallizes in the monoclinic $C2/m$ space group with Ni (S = 1) atoms on honeycomb lattices in the ab-planes. Each Ni atom is octahedrally coordinated by six S atoms, with P atoms situated between the 2D sheets of NiS_6 that form the vdW gap along the c-axis with an interlayer spacing of ≈ 0.636 nm.[2,16] $NiPS_3$ is known to magnetically order at a transition temperature of $T_N = 155$ K; ferromagnetic zig-zag chains form with moments parallel to the a-axis and antiferromagnetically coupled along the b-axis, with a small out of plane component.[16,21]

Figure 1c,e show representative RIXS spectra for bulk and three-layer (3L) $NiPS_3$, respectively. Spectra were collected at the peak of the Ni L_3-edge XAS $E_i = 853$ eV, corresponding to $2p_{3/2}$ to $3d$ electronic transitions. We concentrate on the low energy region $E_{loss} = 0.2 \rightarrow 2.15$ eV that contains excitations within the NiS_6 multiplet. The bulk and three-layer (3L) spectra are qualitatively similar except for an overall energy broadening and softening that is readily visible in the 3L data (Figure 1b). While the qualitative similarity between bulk and 3L spectra is consistent with the fact that there are no drastic structural reconstructions upon exfoliation, the apparent broadening and softening indicates a change in the electronic structure of $NiPS_3$ with thickness.

In order to elucidate the origin of this change, we first concentrate our analysis on the bulk spectra and identify all relevant features. We found that a minimum of six Gaussian modes were required to fit the bulk data, labeled A - F in Figure 1c, with minimum energy widths fixed by the experimental energy resolution ($\approx$ 55meV FWHM). Each of these features can be identified as an excitation within the electronic multiplet of trigonally distorted NiS_6 octahedra (**Figure** 2a; Figure SV, Supporting Information). The center of mass positions of the two bulk peaks are assigned to the $t_{2g} \rightarrow e_g$ (d-d) excitations of $^3T_{2g}$ and $^3T_{1g}$ symmetry, respectively, in good agreement with optical measurements.[17, 22] The trigonal distortion introduces a D_{3d} symmetry which splits $^3T_{2g} \rightarrow {}^3A_{1g} + {}^3E_g$ (peaks B & C) and $^3T_{1g} \rightarrow {}^3A_{2g} + {}^3E_g$ (peaks E & F), in agreement with Raman and optical measurements.[22,23] Access

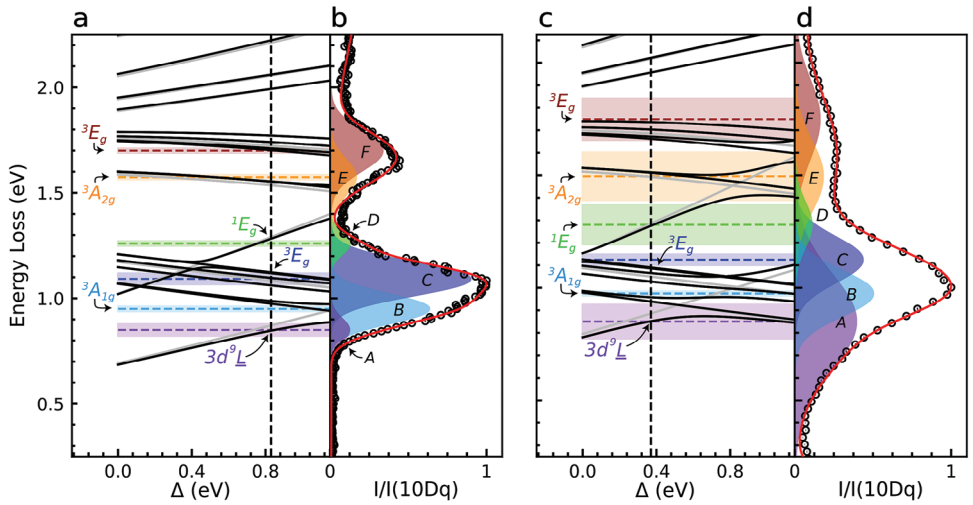

Figure 2. Calculated energy levels of the NiS_6 multiplet ligand-field model as a function of Δ for bulk (a) and 3L $NiPS_3$ (c) compared to normalized experimental spectrum (b, d, respectively). Fixed model parameters are listed in Table 1 and in Supporting Information.[25] In (a,c), black and gray lines show energy levels calculated with and without SOC, respectively. Symmetry labels adapted from a calculation without SOC. Horizontal dashed lines and shaded regions show E_{loss} value and error bars of fitted peaks in rightmost panel, respectively. Vertical dashed line indicates best fit at Δ = 0.83 eV for bulk and Δ = 0.37 eV for 3L $NiPS_3$.

to spin-flip ($\Delta S \neq 0$) excitations in the RIXS cross-section leads us to assign peak D ^1E_g symmetry as the next highest excited state above $^3T_{2g}$ in a $3d^8$ system. Lastly, peak A is assigned to a charge transfer excitation with $3d^9\underline{L}^1$ character, where $\underline{L}^n$ denotes n ligand holes. The 800 meV energy scale of this peak indicates a small charge transfer energy in $NiPS_3$. We verify these peak assignments through the application of the NiS_6 multiplet ligand-field model described below. We note that since our incident energy was tuned to the peak of the Ni L_3-edge XAS, our measurements were not sensitive to the sharp 1.47 eV peak reported in Ref. [24].

We now bring our attention to the spectra collected on the exfoliated samples, and in particular, the 3L sample. Following the fitting procedure from the bulk spectra, we again fit six Gaussian modes; however, Empirically fitting the 3L spectra to a minimum of six Gaussian peaks resulted in two scenarios of equally good fit quality. In order to address the width of peak A, we explore the two fitting scenarios for the 3L spectra. In scenario one, the widths of all peaks were held fixed at the experimental resolution; this fit converged with a systematic softening of all peaks between the bulk and 3L data sets. In scenario two, the FWHM of peak A was allowed to relax, while peaks B - D were fixed to the experimental resolution, and peaks E - F were fixed to the bulk fitted FWHM to experimental resolution ratio; this fit converged with minimal softening of all peaks, but systematic broadening and increased intensity attributed to peak A. We found that peak energies extracted from scenario one could only be reproduced within physically meaningful parameters using a *negative charge transfer energy*, while scenario two is reproduced with a small *positive charge transfer energy*.[25] A negative charge transfer energy for the 3L sample implies a zero-crossing of the charge transfer energy as a function of thickness between bulk and 2D exfoliated samples. We rule out such a transition based on the smooth evolution of thickness dependent RIXS data and Raman spectra.[23]

The full details of each fitting scenario to the 3L spectrum, including details of the bulk spectrum fitting, can be found in the Supporting Information.[25]

Fits for scenario two are shown in Figure 1e, while Figure 1d summarizes the centroids of the fitted peaks for the various sample thicknesses measured. Minimal differences were found between the bulk and 60L, placing a lower limit on bulk behavior for exfoliated $NiPS_3$ at ≈ 38 nm. From bulk to 3L, peaks B - F vary slightly in E_{loss}. We find a broadening in the FWHM of peak A by 360(50) meV over the bulk data that suggests a change in the charge transfer energy in few-layer samples. Furthermore, the observed systematic broadening of excitations signifies an electronic structure intricately connected to sample thickness in $NiPS_3$.

3. Theoretical Analysis

Having identified a clear empirical trend, we perform a thorough fit of the experimental data for paramagnetic $NiPS_3$ using a high-fidelity multiplet ligand-field model (MLFM) in the basis of symmetry-adapted linear combinations of ligand orbitals.[26] Crucially, we use rigorously converged parameter-free solutions of the Schrödinger equation to physically guide our search of the MLFM parameter space. Our MLFM model includes Slater-Condon parameters($F^{0,2,4}_{dd}$, $F^{0,2}_{pd}$, $G^{1,3}_{pd}$), covalent hopping integrals between S 3p- and Ni 3d- orbitals, $pd\sigma$ and $pd\pi$, S 3p- orbital level splitting, $T_{pp} = pp\sigma - pp\pi$, cubic crystal field (10Dq) and trigonal distortion δ, Ni 3d-3d and 2p-3d on-site Coulomb interactions U_{dd} and $U_{pd} = 1.2\,U_{dd}$, and charge transfer energy Δ. The values of the transition metal-ligand ($pd\sigma$, $pd\pi$) and ligand–ligand ($pp\sigma$, $pp\pi$) hopping integrals for bulk and monolayer geometries are calculated independently by self-consistently converging to the electronic ground state of the nonmagnetic configuration of $NiPS_3$

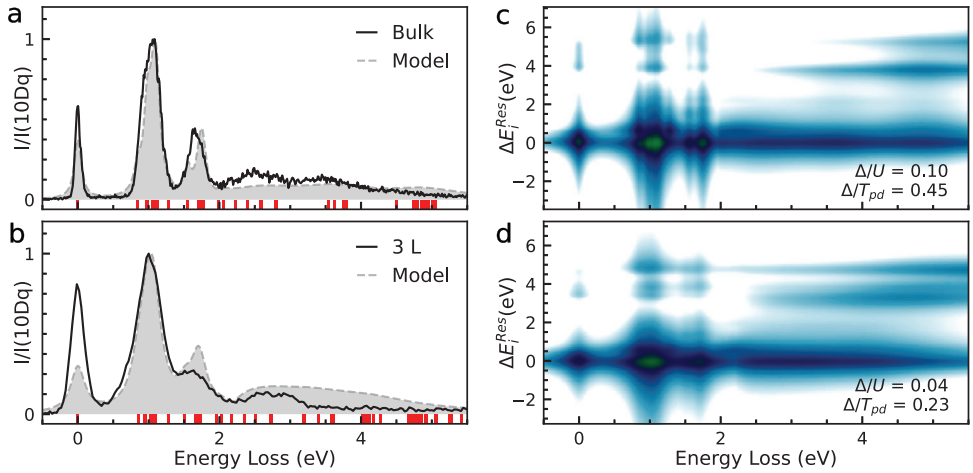

Figure 3. Normalized Ni L_3 RIXS spectra for bulk (a) and 3L (c) $NiPS_3$ with MLFM model from parameters in Table 1 and in Supporting Information.[25] c,d) Simulated RIXS map as a function of incident energy from resonance (ΔE_i^{Res}) and E_{loss}. Δ/T_{pd} and Δ/U parameterize the hybridization and charge transfer characters, respectively. Red bars indicate the eigenvalues of the initial state Hamiltonian obtained from the analysis in Figure 2.

using Density Functional Theory (DFT). We employ a substantial plane wave energy cutoff of more than 3,400 eV, sample the Brillouin zone such that all energies are converged to within less than 0.001 eV, and use correlation-consistent pseudopotentials obtained from fully many-body ab initio calculations.[38] We then generate maximally-localized Wannier functions (MLWF) which span a substantial subspace of the rigorously converged DFT ground states, and use the resulting tight-binding inter-orbital expectation values to solve for the hopping integrals within the two-center linear combination of atomic orbitals approximation.[25]

We carried out a search of the remaining parameter space for Δ, $10Dq$, and $F_{dd}^{0,2,4}$ by minimizing the difference between calculated energies peaks *A* - *F* while keeping $F(G)_{pd}$ fixed to 80% of their atomic Hartree-Fock values.[25,27]. For initial comparisons of this model to our data, we used physically meaningful parameters for octahedrally coordinated NiS_6.[28–30] Figure 2a,c shows the calculated energy levels for a NiS_6 cluster as a function of the charge transfer energy Δ using fixed parameters that give the best agreement between measured and calculated peak energies for bulk and 3L $NiPS_3$, respectively.[25] Previous optical and X-ray absorption (XAS) studies classified $NiPS_3$ as a negative charge transfer insulator,[17] while more recent RIXS and XAS measurements indicate a positive charge transfer gap.[24,31] We find that, for bulk $NiPS_3$, a small positive $\Delta = 0.83$ eV was necessary to give an accurate match to the data; for 3L $NiPS_3$, the charge transfer gap decreases, and accordingly, the best match to the data is obtained with $\Delta = 0.37$ eV.

In **Figure** 3a,b, we show RIXS spectra calculated using the open-source toolkit EDRIXS[32] compared to the experimental data. Intensities were normalized to the nominal $10Dq$ line. Covalent hopping integrals, $pd\sigma$ and $pd\pi$, as well as T_{pp} were fixed to those obtained from ab initio calculations of the nonmagnetic configuration (**Table 1**) while Δ was allowed to vary. To account for broadening of excitations not captured by our multiplet ligand-field model and facilitate better comparison with experimental data, the calculated spectra were broadened by increasing the final-state lifetime above 2 eV in E_{loss}. We can reproduce the observed broadening and softening of NiS_6 multiplet excitations in the 3L spectrum by a decrease in charge transfer energy and transition metal-ligand hopping integrals, as parameterized by Δ/T_{pd}, and Δ/U, where $T_{pd} = -\sqrt{3}pd\sigma$ and on-site $3d$ Coulomb repulsion $U = F_{dd}^0 + \frac{4}{49}(F_{dd}^2 + F_{dd}^4)$[26,33]: $\Delta/T_{pd} = 0.45$ and $\Delta/U = 0.10$ in bulk, and $\Delta/T_{pd} = 0.23$ and $\Delta/U = 0.04$ in 3L.

Table 1. Fixed values in eV of hopping integrals extracted from ab initio calculations of the nonmagnetic configuration. Charge transfer energy Δ, and intra-orbital Coulomb repulsion $U = F_{dd}^0 + \frac{4}{49}(F_{dd}^2 + F_{dd}^4)$ extracted from RIXS modeling.[26,33]

	$pd\sigma$	$pd\pi$	$pp\sigma$	$pp\pi$	T_{pp}	Δ	U
Bulk	−1.07	0.67	0.89	−0.09	0.98	0.83	8.3
3L	−0.93	0.46	0.62	−0.01	0.63	0.37	8.3

We determine that the underlying mechanism responsible for the significant change in the RIXS signal with thickness is predominantly electronic rather than structural in origin, though the lattice constant is slightly overestimated in the PBE-optimized monolayer. We find that as $NiPS_3$ gets thinner, metal-ligand π-hopping is reduced ($pd\pi$ decreases) due to the removal of π-like interlayer vdW interactions. The same effect also causes $pd\sigma$ and T_{pp} to change significantly because of the mixed σ- and π-bonding character present in the sp_3-hybridized phosphorus atoms that bridge the NiS_6 clusters. In the context of our MLWFs, this is reflected in a change in the largest tight-binding energies used to solve for $pd\sigma$ and $pd\pi$ (Figure 1b).[25]

The combination of RIXS measurements and ab initio calculations constrain the electronic ground state that underlies the magnetic properties of $NiPS_3$. In **Figure** 4c, we investigate the change in the ground state character of $|\Psi_g\rangle = \alpha\,|3d^8\rangle + \beta\,|3d^9\underline{L}^1\rangle + \gamma\,|3d^{10}\underline{L}^2\rangle$ extracted from our multiplet ligand-field model as a function of T_{pp} and Δ/T_{pd}. We find a negligible contribution from the $|3d^{10}\underline{L}^2\rangle$ state and nearly equal populations of the $|3d^8\rangle$ and $|3d^9\underline{L}^1\rangle$ states. In bulk, $|\alpha|^2/|\beta|^2 = 1.18$, and in 3L, $|\alpha|^2/|\beta|^2 = 1.3$, implying a small increase in the magnitude of the paramagnetic Ni moment. As shown in Figure 4c, this

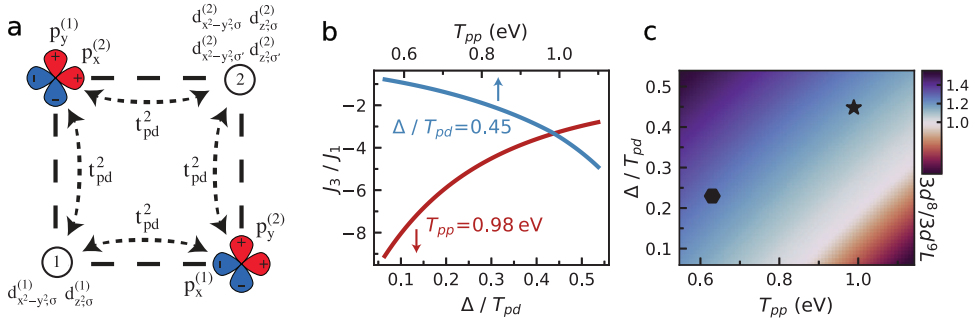

Figure 4. a) Sketch of the nearest-neighbor superexchange process between $d_{x^2-y^2}$ and d_{z^2} orbitals on Ni sites (1,2), mediated by p_x/p_y orbitals on S. b) Calculated change in J_3/J_1 as function of T_{pp} (top-axis) and Δ/T_{pd} (bottom-axis) for fixed bulk values of Δ/T_{pd} and T_{pp}, respectively. c) Calculated ground state ratio of $|3d^8\rangle/|3d^9\underline{L}^1\rangle$ as a function of T_{pp} and Δ/T_{pd}. Star and hexagon points indicate bulk and 3L values of T_{pp} and Δ/T_{pd}, respectively.

minimal change is accounted for by the dependence of the ground state character on both the hybridization Δ/T_{pd} and T_{pp}. While an increased transition metal-ligand hybridization tends to enhance the $|3d^9\underline{L}^1\rangle$ character, this is offset by the reduction in the ligand–ligand hybridization T_{pp}.

Despite the small change in ground state character, the large change in hybridization and hopping parameters influences the magnetic exchange interactions. Using the parameters obtained from our RIXS measurements and ab initio modeling, we compute the superexchange interactions up to the third-nearest neighbor within a sixth order cell-perturbation.[30,34,35] The first J_1, second J_2, and third J_3 nearest neighbor expressions are given by the second order perturbation terms for the $|3d^9\underline{L}^1\rangle$ states, and fourth and sixth order terms for the $|3d^8\rangle$ states;[30] Figure 4a shows the first-nearest neighbor superexchange pathway for the $|3d^8\rangle$ configuration, while a detailed description of all these expressions is given in the Supporting Information.[25] In bulk $NiPS_3$, we find $J_1^B \approx -3.6$ meV, $J_2^B \approx 0.17$ meV, and $J_3^B \approx 12$ meV, in excellent agreement with recently reported values from inelastic neutron scattering.[18,21] The decrease in T_{pp} and Δ/T_{pd} leads to an overall enhancement of $J_1^{3L} \approx -4.2$ meV, a vanishing J_2^{3L}, and decrease in $J_3^{3L} \approx 7.3$ meV. In Figure 4b, we summarize the dependence of J_3/J_1 on T_{pp} and Δ/T_{pd}. We find that J_1 is dominated by the $|3d^9\underline{L}^1\rangle$ state, while J_2 and J_3 are dominated by the $|3d^8\rangle$ state. Thus, the decrease in T_{pp} is directly responsible for an increased $|3d^9\underline{L}^1\rangle$ contribution to J_1. As a consequence of the overall reduction in the *average* exchange interaction strength, the magnetic transition temperature is expected to be reduced in few-layer samples compared to bulk samples. Furthermore, the decrease in J_3/J_1 from -3.3 in bulk to -1.7 in 3L, positions 3L $NiPS_3$ closer to a phase boundary between the stripy AFM phase and a spiral ordered phase.[36] It is likely that, in the 2D limit, $NiPS_3$ is driven into a highly frustrated regime on this phase boundary.

4. Conclusion

In summary, we used RIXS to access the electronic ground state properties of an exfoliated, correlated antiferromagnet in the 2D limit. We found that the electronic energy scales associated with Ni-S hybridization, and consequently the magnetic exchange interactions, are altered in a non-trivial way though the modification of interlayer energy scales upon exfoliation of $NiPS_3$ despite minimal structural changes. Our findings demonstrate that magnetic exchange parameters determined from measurements on bulk materials are not applicable in the 2D limit, as interlayer interactions, absent in 2D, affect intralayer ones. The underlying electronic mechanism we have identified points to the possibility of controlling magnetic interactions in strongly correlated van der Waals heterostructures by tuning interfacial energy scales toward the design of the next generation of 2D strongly correlated magnetic materials.

5. Experimental Section

Crystal Growth: Single crystal samples of $NiPS_3$ were grown by vapor transport, following previously published methods.[16,18] Stoichiometric quantities of metallic Nickel (99.994% purity), crystalline Phorphorus (99.999% purity) and Sulfur (99.999% purity), were added to a quartz tube in an argon-filled glovebox. The quartz tube was then evacuated, sealed, and placed in a two-zone furnace and heated to 700 °C/750 °C over 6 h; the furnace was held at this temperature gradient for 2 days, and cooled to 670 °C/620 °C over 8 h and held for an additional 16 days. After a total of 18 days in the furnace, samples were cooled to room temperature over 8 h. The crystals formed were shiny gray metallic and had hexagonal motif characteristic of $NiPS_3$.

Exfoliated Sample Preparation: Bulk $NiPS_3$ was exfoliated using conventional scotch-tape methods[2] and deposited either onto a blank SiO_2 substrate or onto a SiO_2 substrate pre-treated with a patterned Copper (Cu) grid. Sample layer count was determined using a combination of atomic-force microscope thickness measurements and optical contrast with SiO_2 substrate. See Supporting Information and Figure SII (Supporting Information) for more details.[25] The patterned Cu grid consisted of 100 μ m × μ m SiO_2 cells separated by 200 μ m of 50 *nm* thickness Cu (Figure SIb,c, Supporting Information).[25] The 3L sample was deposited onto a blank SiO_2 substrate and was later patterned with a Cu fiducial marker using electron-beam lithography (Figure SIa, Supporting Information), again with a Cu thickness of 50 *nm*.[25] In both cases, Cu was chosen as a material that could provide a fluorescence contrast to SiO_2 in the soft X-ray regime. This fluorescence contrast proved invaluable in locating small samples whose signals were weak under an X-ray beam. The Cu grid proved a useful method for locating sample(s) as a unique grid scheme could be defined for each chip if the orientation of each chip remained consistent; however, the fiducial marker had the advantage of being visible by eye, resulting in unequivocal sample location and removing the requirement of a grid scheme. Exfoliated samples were spin coated with a PMMA protective layer and stored in an Ar atmosphere to prevent degradation.

RIXS Measurements: Room temperature RIXS measurements on exfoliated flakes were carried out on the PEAXIS beamline at BESSY II.[37] The PMMA coatings were removed immediately prior to loading the samples into the RIXS vacuum chamber via washing with acetone and isopropyl alcohol. All samples chosen for measurement had lateral dimensions larger than, or comparable to, the 15 (H) μ m x 4 (V) μ m x-ray beam spot size at the PEAXIS beamline. A horizontal scattering geometry of $2\theta = 90°$ was used with an ≈ 235 meV energy resolution (full width at half max, FWHM) using linear horizontal polarization and specular geometry. Spectra were collected in 30 min segments to minimize sample exposure to the X-ray beam. It was noted here that the 7 L spectra only was collected with marginally better instrumental resolution of ≈ 190 meV. Bulk $NiPS_3$ RIXS measurements were carried out on the SIX beamline at NSLS II with identical scattering geometry, but with an ≈ 55 meV energy resolution FWHM. The main resonance peak at the Ni L_3-edge was chosen via X-ray absorption spectroscopy (XAS) preformed on-site, prior to each RIXS measurements.

Supporting Information

Supporting Information is available from the Wiley Online Library or from the author.

Acknowledgements

The authors thank Mark Dean for helpful discussions and comments on this manuscript. The authors also thank Naiyuan J. Zhang and Erin Morissette for their guidance and consultation on pattern fabrication. M.F.D. and K.W.P. were supported by the National Science Foundation under grant no. OMA-1936221. A.D.L.T. was supported by the U.S. Department of Energy, Office of Science, Office of Basic Energy Sciences, under Award Number DE-SC0021. D.S. and B.R. were supported by the U.S. Department of Energy, Office of Science, Basic Energy Sciences, Materials Sciences and Engineering Division, as part of the Computational Materials Sciences Program and the Center for Predictive Simulation of Functional Materials, while A.L. was supported by the Brown University Diversity Fellowship. RIXS measurements were carried out at the U41-PEAXIS beamline at the BESSY II electron storage ring operated by the Helmholtz-Zentrum Berlin für Materialien und Energie. This research was conducted using the computational resources of the National Energy Research Scientific Computing Center under Contract No. DE- AC0205CH11231, which is a U.S. Department of Energy Office of Science User Facility, as well as resources and services at the Center for Computation and Visualization, Brown University.

Conflict of Interest

The authors declare no conflict of interest.

Data Availability Statement

The data that support the findings of this study are openly available in Zenodo at https://doi.org/10.5281/zenodo.10125572 , reference number 10125572.

Keywords

magnetic van der waals systems, resonant inelastic x-ray scattering, strongly correlated systems

Received: November 14, 2023
Published online: January 28, 2024

[1] J.-G. Park, *J. Phys.: Condens. Matter* **2016**, *28*, 301001.
[2] C.-T. Kuo, M. Neumann, K. Balamurugan, H. J. Park, S. Kang, H. W. Shiu, J. H. Kang, B. H. Hong, M. Han, T. W. Noh, J.-G. Park, *Sci. Rep.* **2016**, *6*, 20904.
[3] K. Kim, S. Y. Lim, J.-U. Lee, S. Lee, T. Y. Kim, K. Park, G. S. Jeon, C.-H. Park, J.-G. Park, H. Cheong, *Nat. Commun.* **2019**, *10*, 345.
[4] N. Sivadas, S. Okamoto, X. Xu, Craig. J. Fennie, D. Xiao, *Nano Lett.* **2018**, *18*, 7658.
[5] C. Gong, L. Li, Z. Li, H. Ji, A. Stern, Y. Xia, T. Cao, W. Bao, C. Wang, Y. Wang, Z. Q. Qiu, R. J. Cava, S. G. Louie, J. Xia, X. Zhang, *Nature* **2017**, *546*, 265.
[6] Y. Tang, K. Su, L. Li, Y. Xu, S. Liu, K. Watanabe, T. Taniguchi, J. Hone, C.-M. Jian, C. Xu, K. F. Mak, J. Shan, *Nat. Nanotechnol.* **2023**, *18*, 233.
[7] F. Hellman, A. Hoffmann, Y. Tserkovnyak, G. S. D. Beach, E. E. Fullerton, C. Leighton, A. H. MacDonald, D. C. Ralph, D. A. Arena, H. A. Dürr, P. Fischer, J. Grollier, J. P. Heremans, T. Jungwirth, A. V. Kimel, B. Koopmans, I. N. Krivorotov, S. J. May, A. K. Petford-Long, J. M. Rondinelli, N. Samarth, I. K. Schuller, A. N. Slavin, M. D. Stiles, O. Tchernyshyov, A. Thiaville, B. L. Zink, *Rev. Mod. Phys.* **2017**, *89*, 025006.
[8] B. Huang, G. Clark, E. Navarro-Moratalla, D. R. Klein, R. Cheng, K. L. Seyler, D. Zhong, E. Schmidgall, M. A. McGuire, D. H. Cobden, W. Yao, D. Xiao, P. Jarillo-Herrero, X. Xu, *Nature* **2017**, *546*, 270.
[9] K. S. Burch, D. Mandrus, J.-G. Park, *Nature* **2018**, *563*, 47.
[10] M. Gibertini, M. Koperski, A. F. Morpurgo, K. S. Novoselov, *Nat. Nanotechnol.* **2019**, *14*, 408.
[11] A. Kitaev, *Annals of Physics* **2006**, *321*, 2.
[12] K. W. Plumb, J. P. Clancy, L. J. Sandilands, V. V. Shankar, Y. F. Hu, K. S. Burch, H.-Y. Kee, Y.-J. Kim, *Phys. Rev. B* **2014**, *90*, 041112(R).
[13] J. Nasu, J. Knolle, D. L. Kovrizhin, Y. Motome, R. Moessner, *Nature Phys* **2016**, *12*, 912.
[14] K. H. Lee, S. B. Chung, K. Park, J.-G. Park, *Phys. Rev. B* **2018**, *97*, 180401.
[15] B. Zhou, Y. Wang, G. B. Osterhoudt, P. Lampen-Kelley, D. Mandrus, R. He, K. S. Burch, E. A. Henriksen, *J. Phys. Chem. Solids* **2019**, *128*, 291.
[16] A. R. Wildes, V. Simonet, E. Ressouche, G. J. McIntyre, M. Avdeev, E. Suard, S. A. J. Kimber, D. Lançon, G. Pepe, B. Moubaraki, T. J. Hicks, *Phys. Rev. B* **2015**, *92*, 224408.
[17] S. Y. Kim, T. Y. Kim, L. J. Sandilands, S. Sinn, M.-C. Lee, J. Son, S. Lee, K.-Y. Choi, W. Kim, B.-G. Park, C. Jeon, H.-D. Kim, C.-H. Park, J.-G. Park, S. J. Moon, T. W. Noh, *Phys. Rev. Lett.* **2018**, *120*, 136402.
[18] D. Lançon, R. A. Ewings, T. Guidi, F. Formisano, A. R. Wildes, *Phys. Rev. B* **2018**, *98*, 134414.
[19] K. Momma, F. Izumi, *J. Appl. Cryst.* **2011**, *44*, 1272.
[20] B. O. Community, *Blender - a 3D modelling and rendering package*, Blender Foundation, Stichting Blender Foundation, Amsterdam **2018**.
[21] A. R. Wildes, J. R. Stewart, M. D. Le, R. A. Ewings, K. C. Rule, G. Deng, K. Anand, *Phys. Rev. B* **2022**, *106*, 174422.
[22] D. Afanasiev, J. R. Hortensius, M. Matthiesen, S. Mañas-Valero, M. Šiškins, M. Lee, E. Lesne, H. S. J. van der Zant, P. G. Steeneken, B. A. Ivanov, E. Coronado, A. D. Caviglia, *Sci. Adv.* **2021**, *7*, eabf3096.
[23] X. Wang, J. Cao, H. Li, Z. Lu, A. Cohen, A. Haldar, H. Kitadai, Q. Tan, K. S. Burch, D. Smirnov, W. Xu, S. Sharifzadeh, L. Liang, X. Ling, *Sci. Adv.* **2022**, *8*, eabl7707.
[24] S. Kang, K. Kim, B. H. Kim, J. Kim, K. I. Sim, J.-U. Lee, S. Lee, K. Park, S. Yun, T. Kim, A. Nag, A. Walters, M. Garcia-Fernandez, J. Li, L. Chapon, K.-J. Zhou, Y.-W. Son, J. H. Kim, H. Cheong, J.-G. Park, *Nature* **2020**, *583*, 785.
[25] See supporting information for details on sample preparation and preservation, additional details about the exact diagonalization calculations as well as further information about the analysis and fitting of the rixs spectra, details of the ab initio calculation method-

ology in obtaining mlwfs, and tm-l and l-l hopping parameters, and detailed description of the superexchange expressions.

[26] M. W. Haverkort, M. Zwierzycki, O. K. Andersen, *Phys. Rev. B* **2012**, *85*, 165113.

[27] G. Ghiringhelli, M. Matsubara, C. Dallera, F. Fracassi, R. Gusmeroli, A. Piazzalunga, A. Tagliaferri, N. B. Brookes, A. Kotani, L. Braicovich, *J. Phys.: Condens. Matter* **2005**, *17*, 5397.

[28] A. E. Bocquet, T. Mizokawa, T. Saitoh, H. Namatame, A. Fujimori, *Phys. Rev. B* **1992**, *46*, 3771.

[29] S. R. Krishnakumar, D. D. Sarma, *Phys. Rev. B* **2003**, *68*, 155110.

[30] K. Takubo, T. Mizokawa, J.-Y. Son, T. Nambu, S. Nakatsuji, Y. Maeno, *Phys. Rev. Lett.* **2007**, *99*, 037203.

[31] M. Yan, Y. Jin, Z. Wu, A. Tsaturyan, A. Makarova, D. Smirnov, E. Voloshina, Y. Dedkov, *J. Phys. Chem. Lett.* **2021**, *12*, 2400.

[32] Y. Wang, G. Fabbris, M. P. M. Dean, G. Kotliar, *Comput. Phys. Commun.* **2019**, *243*, 151.

[33] Y. Shen, J. Sears, G. Fabbris, J. Li, J. Pelliciari, I. Jarrige, X. He, I. Bozovic, M. Mitrano, J. Zhang, J. F. Mitchell, A. S. Botana, V. Bisogni, M. R. Norman, S. Johnston, M. P. M. Dean, *Phys. Rev. X* **2022**, *12*, 011055.

[34] J. H. Jefferson, H. Eskes, L. F. Feiner, *Phys. Rev. B* **1992**, *45*, 7959.

[35] H. Eskes, J. H. Jefferson, *Phys. Rev. B* **1993**, *48*, 9788.

[36] J. Fouet, P. Sindzingre, C. Lhuillier, *Eur. Phys. J. B* **2001**, *20*, 241.

[37] C. Schulz, K. Lieutenant, J. Xiao, T. Hofmann, D. Wong, K. Habicht, *J. Synchrotron Rad.* **2020**, *27*, 238.

[38] A. Annaberdiyev, G. Wang, C. A. Melton, M. C. Bennett, L. Shulenburger, L. Mitas, *The Journal of Chemical Physics*, **2018** *149*. https://doi.org/10.1063/1.5040472